HAL open science

Combustion and pollutant emission characteristics of argan nut shell (ANS) biomass

Yassine Rahib, Toufik Boushaki, Brahim Sarh, Jamal Chaoufi

▶ **To cite this version:**

Yassine Rahib, Toufik Boushaki, Brahim Sarh, Jamal Chaoufi. Combustion and pollutant emission characteristics of argan nut shell (ANS) biomass. Fuel Processing Technology, 2021, 213, pp.106665. 10.1016/j.fuproc.2020.106665 . hal-03173858

HAL Id: hal-03173858

https://hal.science/hal-03173858v1

Submitted on 3 Feb 2023

HAL is a multi-disciplinary open access archive for the deposit and dissemination of scientific research documents, whether they are published or not. The documents may come from teaching and research institutions in France or abroad, or from public or private research centers.

L'archive ouverte pluridisciplinaire **HAL**, est destinée au dépôt et à la diffusion de documents scientifiques de niveau recherche, publiés ou non, émanant des établissements d'enseignement et de recherche français ou étrangers, des laboratoires publics ou privés.

Distributed under a Creative Commons Attribution - NonCommercial 4.0 International License

Version of Record: https://www.sciencedirect.com/science/article/pii/S0378382020309565
Manuscript_bba98af1fe14090019b726f6d4010da2

Combustion and pollutant emission characteristics of argan nut shell (ANS) biomass

Yassine Rahib[1, 2, *], Toufik Boushaki[1], Brahim Sarh[1], Jamal Chaoufi[2]

*Corresponding author: yassine.rahib@cnrs-orleans.fr, yassine.rahib@gmail.com;
[1] Institute of Combustion, Aerothermal, Reactivity and Environment (ICARE)-CNRS UPR3021, 45071 Orléans Cedex 2, France.
[2] Laboratory of Electronics, Signal Processing and Modelling Physics, Department of Physics, Ibn Zohr University, 80000 Agadir, Morocco

Abstract

This paper presents an experimental study of argan nut shell (ANS) combustion in a lab-scale furnace. Biomass composition, properties and microstructures were determined. Combustion behaviour, fuel burn rate (FBR), pollutants (CO and NO_x), modified combustion efficiency (MCE) and ash analysis were investigated. A comparison with wood pellets (WP) complying with the ENplus Standard was performed. The impacts of air flow rate and particle sizes on the combustion characteristics were analysed and discussed using three average ANS particle lengths: 5-8 mm, 10-18 mm and 25-30 mm. The results show that the smallest length of ANS particles induced a higher FBR and a regular distribution of the flame shapes compared to the other sizes and to wood pellets. Furthermore, the combustion temperatures, CO emission and MCE values were improved with the highest air flow rate used. CO emission was strongly affected by the operating conditions while NO_x was very low for all selected cases. Elemental ash composition reveals that no ash agglomeration was observed during experiments in terms of alkali index. Moreover, the obtained ash was in the form of powder instead of agglomerated particles. This experimental investigation improves the understanding of the operational characteristics and the combustion effect of ANS biomass.

Keywords: Biomass combustion, argan nut shell, combustion behaviour, fuel burn rate, pollutant emissions, ash analysis.

© 2020 published by Elsevier. This manuscript is made available under the CC BY NC user license
https://creativecommons.org/licenses/by-nc/4.0/

1. Introduction

Nowadays, there is significant interest in biomass feedstock for applications in green energy as these materials represent an abundant, clean and renewable alternative energy resource. In fact, biomass is considered as the fourth largest source of energy following petroleum, coal and natural gas, with a current world demand for energy estimated at 53 EJ [1]. Most applications of this global energy supply concern an assortment of energy needs, including generating electricity, heating homes, cooking purposes and some industrial applications [2]. However, a major part of the rural population in developing countries is dependent on biomass, mainly as traditional fuel for cooking and heating. Agricultural residues are the most widely available biomass materials with a high energy potential. Werther et al. [3] estimated that over three billion tons of agricultural residues are generated world-wide. In addition, this resource is considered to be less controversial than fossil fuels, low cost and thus represents an important energy resource for countries with a massive agricultural production.

The present study concerns the energy recovery of agricultural waste in the Mediterranean basin. Argan is one of the agricultural resources producing this waste during the argan oil production process; most of the waste is generated by the argan nut shell (ANS) [4]. The ANS can be considered as an attractive source of biomass, since it is procurable in abundance and does not contend with food production. The raw materials of ANS used in this work were from the region of Sousse-Massa-Draa (southwestern Morocco) in which the development is based on agricultural activities. The annual production of ANS is estimated at 60 000 tons per year.

Among thermochemical conversion processes, combustion is a promising technology and the most common option for biomass conversion [5]. Fixed-bed combustion is considered a suitable and routine technique to optimize and transform agricultural residues into thermal

energy [6]. Studies on the combustion characteristics of fixed beds of biomass have been reported by many papers. Khlifi et al. [7] studied the combustion of briquettes prepared from olive mill solid wastes in the same reactor as the one used herein. They reported the influence of the binder added to the prepared briquettes on combustion efficiency and pollutant emissions. Khor et al. [8] and Cepic et al. [9] investigated the combustion characteristics of straw in a fixed-bed reactor. Roy et al. [10] reported the combustion and emission results obtained during the burning of four biomass pellets in a prototype pellet furnace. Elmay et al. [11] studied the energy recovery of date palm residues from Tunisia, in a domestic pellet boiler. The combustion parameters such as air flow and fuel particle size have been investigated in the literature. Ryu et al. [12] experimentally investigated the effect of particle size and air flow on the combustion characteristics of four biomass samples by determining equivalence ratio, combustion temperature, ignition and burning rate. Rahib et al. [13] briefly presented the combustion and emission characteristics of raw argan nut shell (ANS) in a fixed-bed reactor. The focus was placed on the relationship between the nourishing tissue of the argan almond and SO_2 emissions. Onabanjo et al. [14] studied the combustion performance of human faeces by determining the combustion temperature, the fuel burn rate and the combustion efficiency. They varied air flows, biomass sizes, bed heights, and fuel ignition mode parameters in order to determine the optimum conditions for converting the faecal biomass into energy. Meng et al. [15] examined the effect of varying corn straw lengths and primary air flow on the combustion characteristics. They suggested that these two parameters directly affect the burning rate, the bed temperature, the combustion emissions and the boiler efficiency. The focus of our experimental research was to identify the conditions that can lead to improved combustion of ANS in biomass combustion installations with ~50 MW output.

To comprehend the combustion process of ANS, the present paper investigates the influence of particle lengths and air flows on combustion quality in a laboratory furnace. To the best of our knowledge, no studies have been reported to date in the literature on the combustion performance of ANS in a laboratory combustor. The first part of this work is a parametric study to analyse the effect of different air flows. Measurements were carried out on raw ANS and three different particle lengths chosen to analyse the size effect on combustion. A comparison with wood pellets was performed. Results include flame structures and stabilities for all the selected samples as well as ash analysis at different running conditions. In view of the absence of ANS combustion studies, this work would be of great interest to biomass combustion studies.

2. Materials and methods

This study uses the ANS as raw biomass for combustion. Physicochemical characterization was checked through ultimate and proximate analyses as well as the energy content measurement. Ultimate analysis was carried out, using a FLASH 2000 CHNS/O analyser (Thermo Scientific), to determine carbon (C), hydrogen (H), oxygen (O), nitrogen (N) and sulphur (S) weight fractions. Proximate analysis was done using a Shimadzu analyser DTG-60 according to the ASTM standard procedures. A more detailed description of the experimental protocol can be found in our previous work [16]. A calorimetric bomb (Parr 2100) was used to measure the high heating value (HHV). The low heating value (LHV) was calculated based on water and ash free contents. The energy density was obtained by multiplying bulk density by the LHV. The empirical formula was computed based on C, H and O content (masse fractions from ultimate analysis). By taking Carbone as reference, the empirical formula of ANS is calculated as $CH_{1.46}O_{0.62}$ (where 1.46 and 0.62 represent H/C and O/C molar ratios). The basic chemical reaction of ANS stoichiometric combustion can be written as:

$$CH_{1.46}O_{0.62} + 1.05\ (O_2 + 3.76\ N_2) \rightarrow CO_2 + 0.73\ H_2O + 3.97\ N_2 + Q\ (heat) \quad (1)$$

This equation was used to determine the theoretical air-fuel ratio.

A scanning electron microscope (SEM) was used to determine the physical nature of raw ANS and ash at different magnifications. The equipment used was a JEOL JSM-IT100 SEM model, connected to a dispersive energy X-ray spectroscopy (EDS) unit which was used to access elemental composition in a semi-quantitative way. To set up this experiment, the tested material was stuck on a thin layer of carbon.

Combustion of the ANS took place in a batch fixed-bed reactor. This device was developed at ICARE-CNRS to investigate the thermochemical conversion process of agricultural biomasses. Fig. 1 shows a schematic diagram of the experimental setup which consists of: (1) an air fan adjusted by a frequency regulator (0-50 Hz), (2) a combustion chamber composed of: a bottom ash recovery, a fixed grate, a rotating leveller, then a confinement where the flame arises, (3) a cyclone connected by a flue pipe from the combustion chamber outlet, (4) a flue gas scrubber.

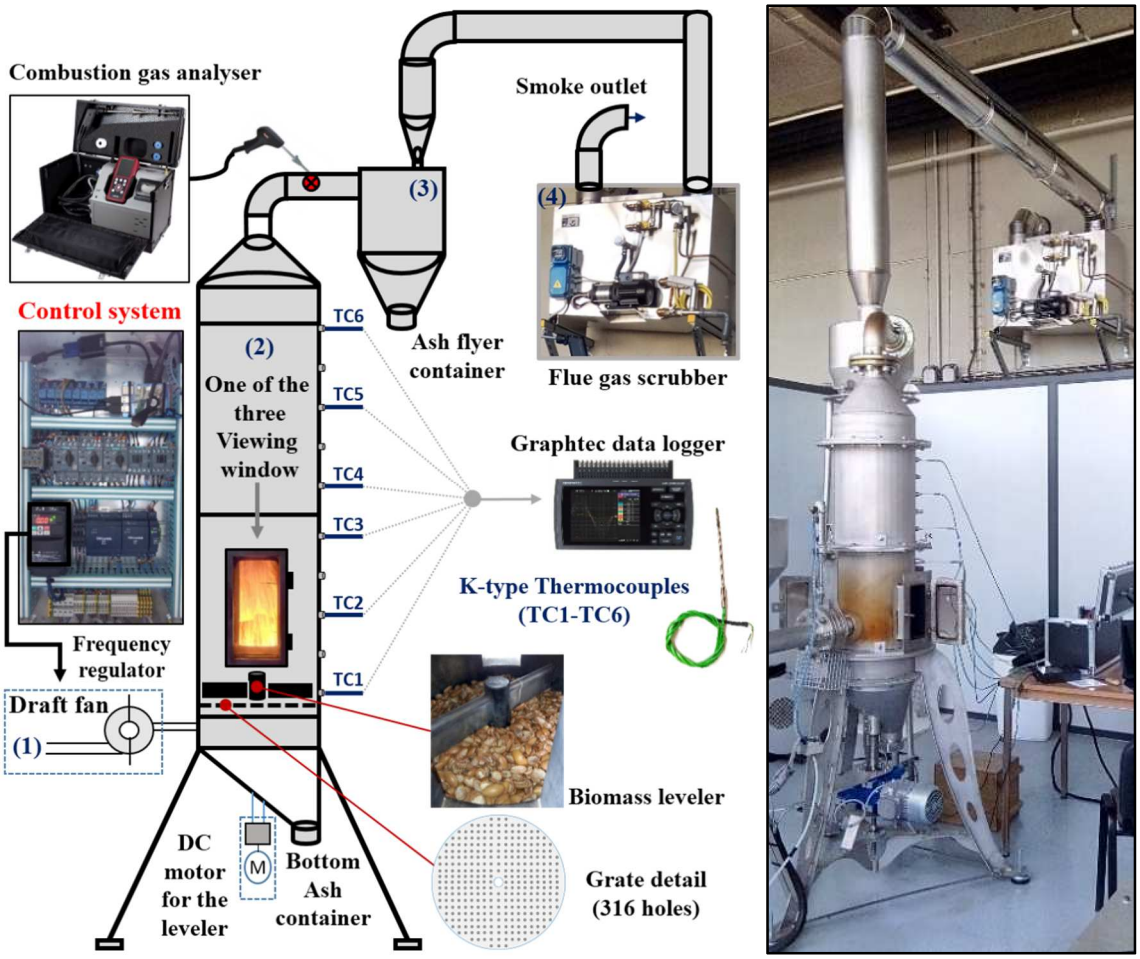

Fig. 1. Experimental combustion setup.

The main components and measuring devices of the experimental rig are also illustrated. The combustion chamber is divided into two compartments. It can be equipped with ten K-type thermocouples inserted into the chamber centre to monitor the variation in flame and maximum temperatures. Table 1 summarizes specific positions of the used thermocouples (TC1-TC6). The temperature profiles were recorded every second by a Graphtec data logger.

Table 1 Positions of the thermocouples along the combustion chamber.

Number	Distance from the grate (mm)
TC 1	55
TC 2	195
TC 3	335
TC 4	455
TC 5	595
TC 6	735

In the experiments, the composition and temperatures of the combustion gases were measured in-situ at the combustion chamber outlet. Before analysing the flue gas, the apparatus was calibrated. All emission profiles were recorded in the steady state zone. The gas analyser used (Kimo KIGAZ 500) incorporates infrared and electrochemical measurement techniques. The maximum response time of this instrument is less than 50 s. Therefore, a sampling duration of 1 min was used to obtain stable values. At the beginning of each experimental test, 1 kg of ANS is placed on the grate. Then, the leveller is switched on to establish homogeneous distribution of the biomass bed. Afterwards, ignition of the biomass is started on the entire surface of the bed using a gas blow torch and a small amount of liquid fuel to promote the onset of combustion. A long-distributed flame throughout the upper surface of the bed indicates a successful ignition and combustion test (see Fig. 2). The air enters from the boiler bottom through the bed into the combustion chamber. The experimental protocol followed is relevant for fixed grate and domestic boilers since (a) this configuration can present the same contact between biomass particles in the bed, (b) the biomass successively undergoes drying, devolatilization and char combustion and (c) geometric and operational configurations relating to the aspect ratios of biomass particles, dimensions of the bed and the flow paths of combustion gases are the same. Thus, some of the investigations made herein could be quantitatively applicable to industrial combustion systems.

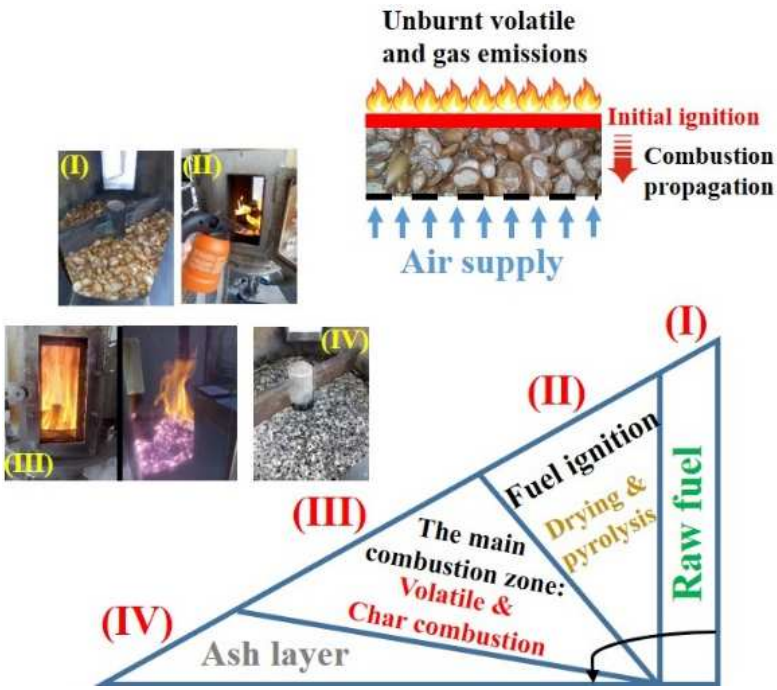

Fig. 2. Experimental procedure of the combustion tests.

The flows used in this study were 36, 72, 108, 144 and 180 $m^3.h^{-1}$ corresponding to 528, 1057, 1585, 2113 and 2642 $kg.m^{-2}.h^{-1}$, respectively (in mass flow). At the end of each combustion test, the remaining ashes (bottom and fly ash) were collected and weighed. The optimum operating conditions for the ANS combustion were determined by varying air flow and particle lengths. The key performance of the process was assessed quantitatively by determining: the modified combustion efficiency (MCE), the fuel burning rate (FBR), the combustion temperatures, the average concentration of the combustion gases and the flame structures.

The MCE under different operating conditions was calculated based on CO and CO_2 emissions as described in equation (2):

$$MCE\ (\%) = CO_2\ (\%) / [CO_2\ (\%) + CO\ (\%)] \quad (2)$$

The FBR ($g\ s^{-1}$) as expressed in equation (3) signifies the time required for complete combustion of the biomass fuel consumed, at the end of each individual experiment, in mixture with air. It indicates the rate of energy released into the system.

$$FBR\ (g\ s^{-1}) = m_f\ (g) / t(s) \quad (3)$$

The FBR can be used to evaluate the biomass bed velocity (BBV) which was calculated by equation (4). Generally, the BBV increases with increase of FBR.

$$BBV\ (mm.s^{-1}) = FBR\ (kg.s^{-1}) / [Bulk\ density\ (kg.m^{-3}) * grate\ area\ (m^2)] \quad (4)$$

The end of each combustion experiment was selected to be the time moment when the temperature recorded from TC1 or TC2 decreased below 250 °C. At each air supply and fuel particle length, the performance criteria were tested in the steady state zone (flaming mode) when there was almost no change in flame temperature.

In order to shed light on the evolution of the combustion gas concentrations and temperature, we studied the impact of excess air on the combustion of ANS. The excess air is determined indirectly by measuring the concentration of unreacted oxygen in the flue gaz. A better approximation of the excess air can be computed using equation 5 [17].

$$\%\ Excess\ Air = \frac{O_2 - {}^{\%CO}/_{2}}{20.9 - (O_2 - {}^{\%CO}/_{2})} * 100 \quad (5)$$

The concentrations of O_2 and CO are obtained from sampling the gas at the combustion chamber outlet. The air factor (λ) and the equivalence ratio (ϕ) are deduced by:

$$\lambda = \frac{\%\ Excess\ Air}{100} + 1\ ;\ equivalence\ ratio\ (ER) = \phi = \frac{1}{\lambda} \quad (6)$$

3. Results and discussion

3.1. Biomass characterization

Energy content, ultimate and proximate analyses of the raw sample are summarized in Table 2. The relatively high moisture content of ANS (9.5%) is in the range of some biomass sources used in thermal conversions [18]. However, the low ash content will positively impact the combustion efficiency and eliminate slag formation in the boiler. The high content of volatiles (61%) is an attractive characteristic that can improve the ignition process during combustion. The carbon and hydrogen contents were found to be 51.3 and 6.32%

respectively. ANS is also listed to have an impressively high heating value (HHV = 18.3 $MJ.kg^{-1}$) despite the significant oxygen content. A critical property of biomass materials is bulk and energetic density, which are linked to storage and transport costs [19]. The values found for these two properties were 596 $Kg.m^{-3}$ and 10.13 $GJ.m^{-3}$ (for bulk and energetic density, respectively). This indicates that ANS can be an excellent candidate for thermochemical conversion [16,19,20]. Moreover, the hardness of ANS makes their storage and transport easier and ensures their long durability. The low values of N and S are a good indicator concerning the release of NO_x and SO_x pollutants to the atmosphere [16]. The theoretical air volume per kg fuel, calculated based on the ultimate analysis of the fuel, was found to be 4.75 $Nm^3.kg^{-1}$. It refers to the amount of air necessary to complete combustion. The stoichiometric air fuel ratio (AFR) was also calculated (6.23 kg-air/kg-fuel) to identify the amount of air and fuel required for complete combustion.

Table 2 ANS biomass properties.

Photograph of the raw ANS particles	Ultimate analysis [a] (%)				
	C	H	O	N	S
	51.33	6.32	42.345	0.005	n.d.
	Proximate analysis [b] (%) and bulk density (BD)				
	M	VM	FC	ash	BD
	9.5	61	28	1.5	596
	Energy content [b] and stoichiometric calculation [a]				
	LHV	ED	Equivalent formula	Stoichiometric air ($Nm^3.kg^{-1}$)	AFR
	17	10.13	$CH_{1.46}O_{0.62}$	4.75	6.22

n.d.: not detected, M: moisture, VM: volatile matter, FC: fixed carbon, BD: bulk density ($Kg.m^{-3}$), LHV: low heating value ($MJ.kg^{-1}$), ED: Energetic density ($GJ.m^{-3}$), AFR: air fuel ratio (kg-air / kg-fuel).
[a] dry ash free basis, [b] as received basis

The photo in Fig. 3 shows the morphological characteristics of the raw sample. It was not subjected to any handling apart from natural dehydration in atmospheric air to eliminate external moisture. It can be seen that the ANS presents a polygonal organization composed of smooth and homogeneous zones indicated by the letters (x) and some roughness on its external surface (y). Damage to the external area of the material at the end of some particles (z) was observed, perhaps because of the fruit kernel crushing process. The SEM-EDS results

show that ANS is mainly composed of carbon (C) and oxygen (O). Minor amount of Al and Si were detected in the cracked zone (zone 001). Fig.3 includes the EDS analysis results.

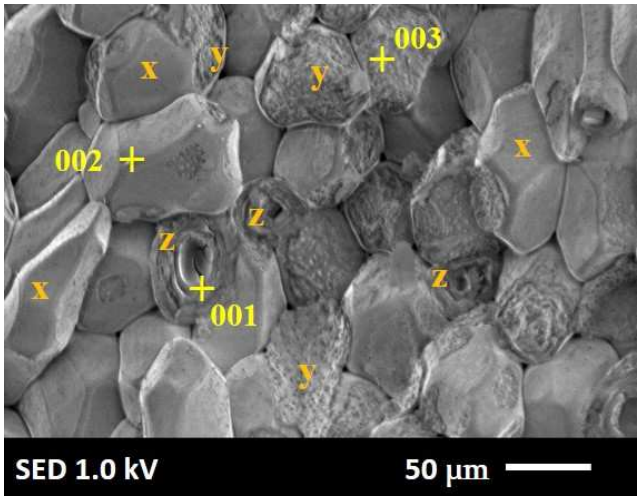

	O	C	Al	Si
001	40.48	56.26	1.50	1.76
002	19.13	80.87		
003	33.98	66.02		
Average	31.20	67.72	1.50	1.76
Deviation	10.94	12.39	0.00	0.00

Fig. 3. Scanning electron microscope image and additional elemental analysis of the outer surface of ANS.

Fig. 4 shows the microstructure of the ash content of raw ANS. This material was obtained by the LOI (loss on ignition) method, i.e. raw ANS was combusted at 850 °C during three hours in a muffle oven according to the EN NF M03-003 procedure to eliminate all carbon content [21]. The morphology of the ash reveals the existence of small agglomerates (not significant) and the amorphous shape of particles (partially molten particles: spot 003). As we can see from elemental analysis, the ash contains mainly oxygen. The amount of carbon was very low and a significant amount of potassium K was identified (spot 1 and 2). Other major elements, in decreasing order, such as Mg, Na, P, Ca, S, Al and Si were detected.

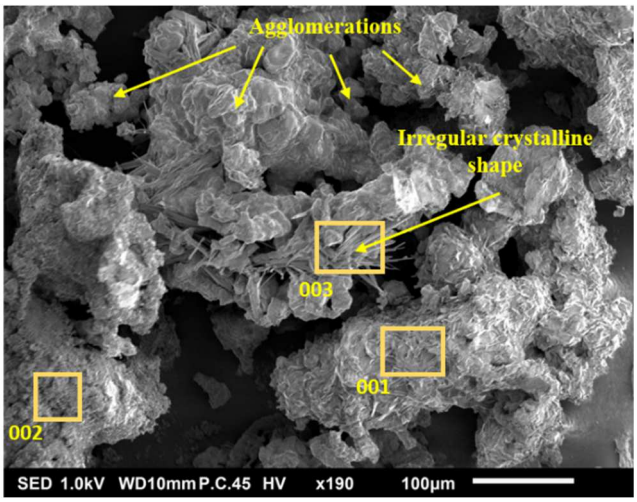

EDS	001	002	003	Av	S. Dv.
P	3.2	0.5	11.2	4.9	5.59
K	28.3	25.5	13.0	22.2	8.1
O	44.9	36.1	41.0	40.7	1.2
C	6.2	3.7	4.2	4.7	1.3
Na	6.4	0.9	19.8	9	9.7
Mg	1.4	27.6	3.4	10.82	14.6
Al	-	-	1.5	1.5	0
Si	1.6	1.12	0.6	1.1	0.5
S	0.37	-	3.3	1.8	2.1
Ca	7.67	4.47	1.8	4.6	2.9

Av: average, S. Dv.: standard deviation

Fig. 4. SEM-EDS analysis of ANS ash obtained by LOI method.

3.2. Visual observation of the combustion

A general trend of combustion behaviour in fixed beds was observed. Fig. 5 shows the flame images from the videos of ANS as a function of three air flows and the particle sizes. This flame represents the combustion of pyrolysis gas during the whole process [22]. The wood pellets (WP) were also included for the purpose of comparison. The higher air flow supply (180 $m^3.h^{-1}$) affected combustion stability, slowed down the combustion process and extinguished the flame (cases LP (large particle) and SP (small particle)). In the RP (raw particle) case, it was noticed that a higher air flow did not extinguish the flame but limited its progress along the combustion chamber. This can be attributed to the presence of broken particles in the raw ANS, which need more oxygen to complete the burning process (see further explanations in section 3.4). In the BP (broken particle) and WP cases, the high air supply did not perturb the flame; the combustion seemed homogeneous, and the flame was very stable. With a lower air flow supply (72 $m^3.h^{-1}$), the flame images in RP, LP, SP, BP and WP showed intense luminosity, which indicates the existence of some soot because of the rich regime of biomass. The luminosity decreased with increasing air flow, since oxygen addition improved the combustion process (fuel lean conditions).

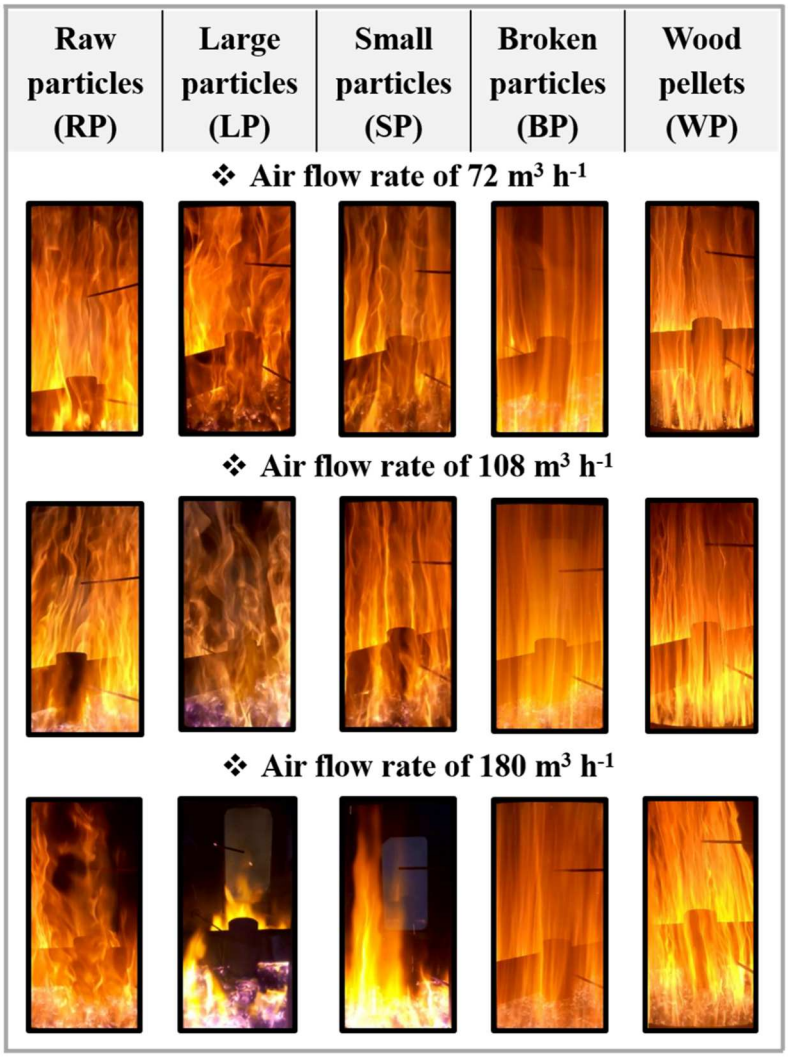

Fig. 5. Images of visible flames from the combustion recording of ANS at different operating conditions and particle sizes. WP are added for comparison.

From a structure and stability point of view, flames in the case of BP under the studied air supply were characterized by a regular shape and a relatively smooth and continuous flame front. This can be explained by the existence of a pre-mixed zone in which the volatile gases released by the broken particles mixed well with the surrounding air. This behaviour is similar to premixed gas combustion as in [23] where the combustion reactions are mainly affected by chemical kinetics. The LP and SP probably take a lot of time to devolatilize [12,24], which contributes to delaying ignition and to a more irregular flame shape. The flame becomes increasingly stable when particle sizes decrease.

3.3. Effect of air flow

The combustion tests of raw ANS samples in varying air flow conditions were performed to analyse the effect of this crucial parameter in achieving the highest combustion performances. Fig. 6a-c reveals a typical flame temperature profile (a), combustion behaviour (b) and combustion gas concentration (c) inside the reactor with a 36 $m^3.h^{-1}$ air supply (528 $kg.m^{-2}.h^{-1}$). The process can be divided into four stages as illustrated in Fig. 6a: (1) start-up (2) steady-state (3) combustion of residual char and (4) switch off. Similar behaviour was identified in the other air supply cases with some oscillation observed in the steady state zone. Fig. 6b illustrates visual observations of the four stages of the combustion process. The steady state zone was found to be characterized by homogenous (flame mode: blackening of bed particles) and heterogeneous (flame was observed during char ignition) combustion behaviour. The combustion of the char heats the bed without significant heat exchange to the bordering flame. The first chute (stage 3) indicates the beginning of flame extinction. Once the volatile flame extinguishes, the ANS bed starts to lose heat, whence the second slopes (stage 4). Fig. 6c shows the gas emission profiles as a function of combustion time. The O_2 concentration decreased swiftly as the combustion process proceeded. This was followed by an increase in CO_2, CO, CH_4 and NO_x (NO + NO_2). The CO_2 content is predominant because of the higher carbon content in ANS. When the biomass flame began to drop (Switch off: char mode), the O_2 concentration began to rise, while CO, CO_2, CH_4, NO_x and SO_2 declined regularly, indicating the end of combustion stage. Generally, the combustion process of ANS was shown to be dominated by the flaming mode. The combustion of the remaining char, after the extinction of the flame, was not a major event [20]. This behaviour was similar to that reported in [25].

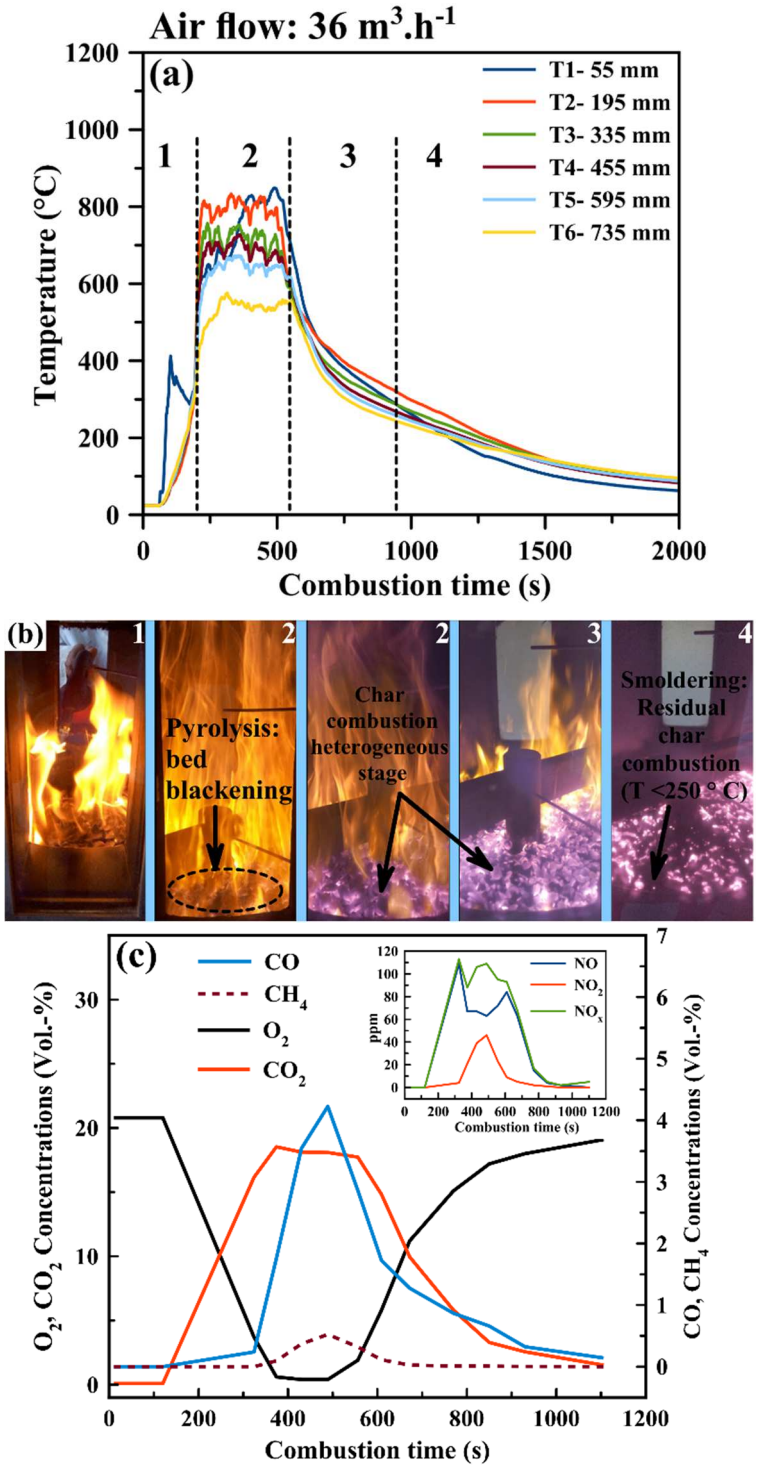

Fig. 6. Typical combustion results: (a) flame temperature (b) visual observation and (c) corresponding combustion gas concentrations (case of 36 $m^3.h^{-1}$ air supply).

Fig. 7a-c illustrates the significant impact of air flow on the combustion process of raw ANS. Calculated equivalence ratios (ER) in the flame zone, (equations 5 and 6), are shown in Fig. 7a.

The bold arrow (dotted line) indicates the theoretical stoichiometric combustion regime. The instantaneous ER measured at different air flow rates (except for 36 $m^3.h^{-1}$) is located in the "sub-stoichiometric" fuel lean zone (ER < 1 at the interval of 300 and 700s) of the transient combustion period. With an air flow supply of 36 $m^3.h^{-1}$, the rich regime appears (ER >1) in the combustion period between 370 and 550s. In this zone, all the oxygen was consumed (temporary oxygen deficiencies: O_2 < 0.1%) and high emissions of CO and CH_4 were observed (see Fig. 6c). Moreover, the intermittent flame zone (ER < 0.45) characterizes the rapid extinguishes of the flame due to convective cooling (when the air flows are not favourable: Fig. 5, air flow rate of 108 $m^3.h^{-1}$). The results in Fig. 7b reveal that the maximum flame temperature (registered by TC1 or TC2) increased progressively with increasing of the air flow until a value of 886 °C corresponding to an air flow of 108 $m^3.h^{-1}$. Beyond this flow rate, the flame temperature decreased with the increase of the air flow. The exhaust gas temperature had the same behaviour, with a maximum value of 767 °C corresponding to the same air flow. Similar behaviour was also observed in the case of FBR, which presented maximum values of 1.39 and 1.43 g s^{-1} for an air flow of 108 and 144 $m^3.h^{-1}$, respectively. The FBR decreased gradually with further increase in the air supply (case of 180 $m^3.h^{-1}$). Fig. 7c reveals that the modified combustion efficiency ranged from 88 to 97% as a function of the studied range of the air flow (36 to 180 $m^3.h^{-1}$). It is shown that MCE increased then decreased with the air flow, with a maximum value (97%) observed at 108 $m^3.h^{-1}$. The BBV presented the same behaviour as FBR with maximum values at 108 and 144 $m^3.h^{-1}$ corresponding to the same air flows. As noted by Khor et al. [8], the combustion temperature and burning rate of straw increased significantly with an increased in air flow velocity until a critical point. Thereafter, they decreased with a further increase in primary air flow due to convective cooling, because the impact of increased convection was stronger than the effect of increased temperature at high flow rate. Onabanjo et al. [14] observed that the combustion

reaction of human faeces rapidly turned off when the air flow exceeded a critical value. They suggested that the excess air flow (unfavourable, i.e. convection by cooling) limits the flame propagation, reduces the combustion temperature and affects the combustion stability.

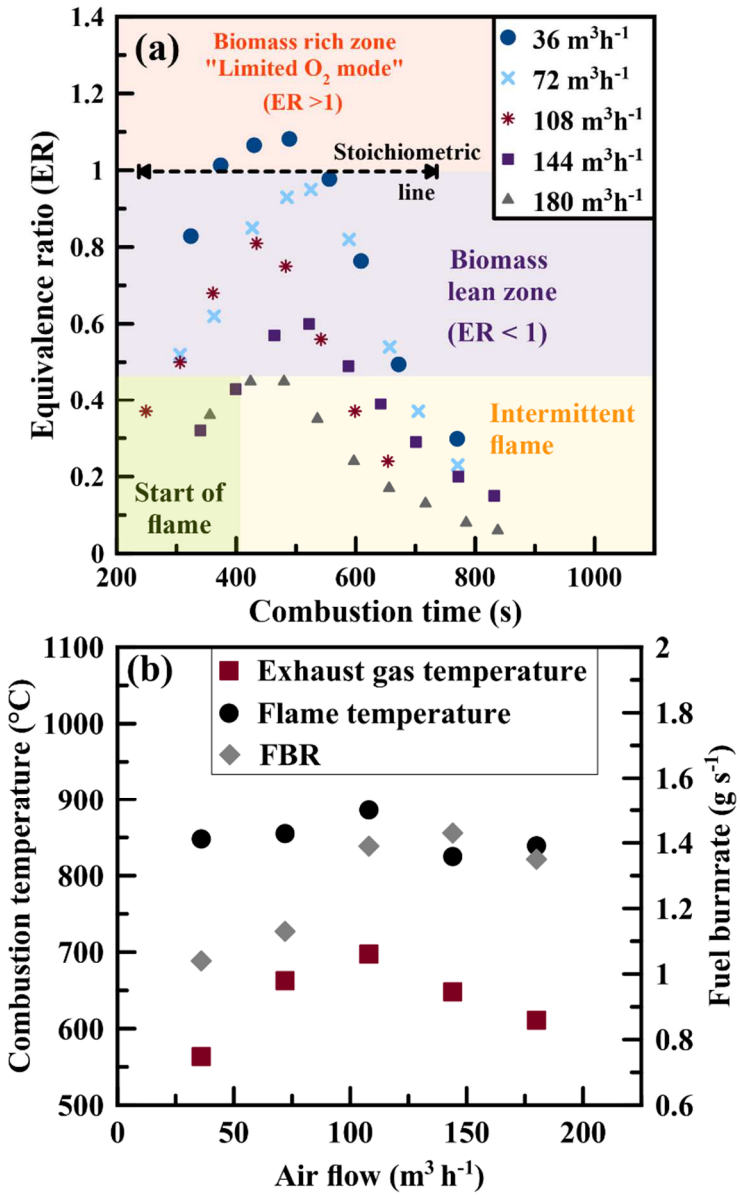

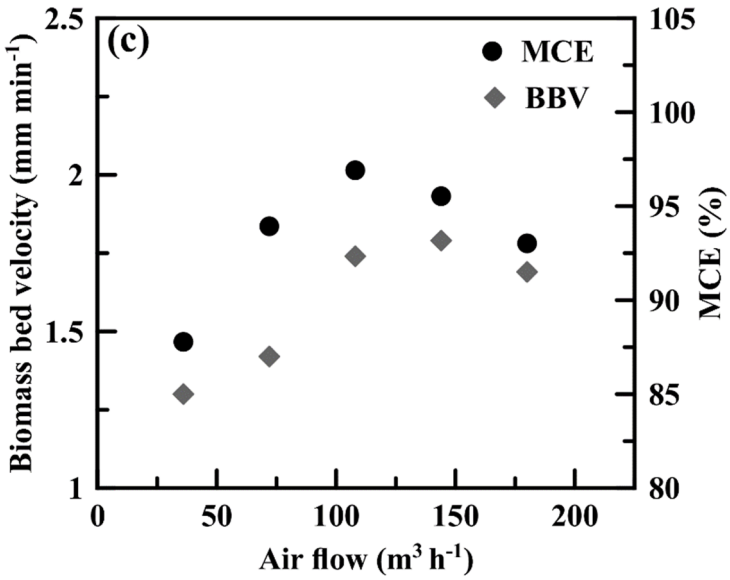

Fig. 7. Influence of the air flow on: (a) equivalence ratio (b) combustion temperature and FBR, (c) BBV and MCE.

Fig. 8 shows the mean pollutant concentration calculated, converted and corrected at 10% O_2 using the following formula, respectively [17] [26] :

$$C_{mean}(ppmv) = \frac{1}{\tau}\int_0^{\tau}[Concentration]_{Exp}(\tau)\,d\tau$$

$$C_{mean}(mg.Nm^{-3}) = C_{mean}(ppmv) * \frac{gram\ molecular\ weight}{molar\ volume} \quad (7)$$

$$[Concentration]_{corrected\ at\ X\%\ O_2} = [Concentration]_{Exp} * \frac{20.9 - X\%O_2}{20.9 - [\%O_2]_{Exp}}$$

where C_{mean} is the mean pollutant concentration; τ is the time of biomass combustion (s); molar volume at STP (0 °C and 1 atm.) = 22.414 l; $X\%O_2$ is the reference oxygen content in % volume and Exp is the measured concentration.

In this Figure, the effect of varying air flow on the combustion process is demonstrated. The CO concentration in the gas was very high ($1.5\ 10^4$ mg.Nm^{-3}) with an air flow of 36 m^3.h^{-1} because of the rich regime of biomass. It decreased progressively on increasing the air flow until a value of 3973 mg.Nm^{-3} corresponding to 108 m^3.h^{-1}. Afterwards, the CO concentration increased gradually at high air excess (144 and 180 m^3.h^{-1}) due to a high amount of unburnt

biomass, resulting in the increase in C char emissions (short residence time of ANS in the combustion zone). The NO_x emissions (calculated based on the measured concentrations of NO and NO_2) were relatively weak (below 140 mg.Nm^{-3} referred to 10% O_2 in the fume (Fig. 8)). This was an expected positive result given the very low nitrogen content (0.005% on dry ash free basis). Emissions of CH_4 decreased from 688 mg.Nm^{-3} at 36 m^3.h^{-1} to 3 mg.Nm^{-3} at 180 m^3.h^{-1}. With a 108 m^3.h^{-1} air supply, the CH_4 value was found to be very low (44 mg.Nm^{-3}).

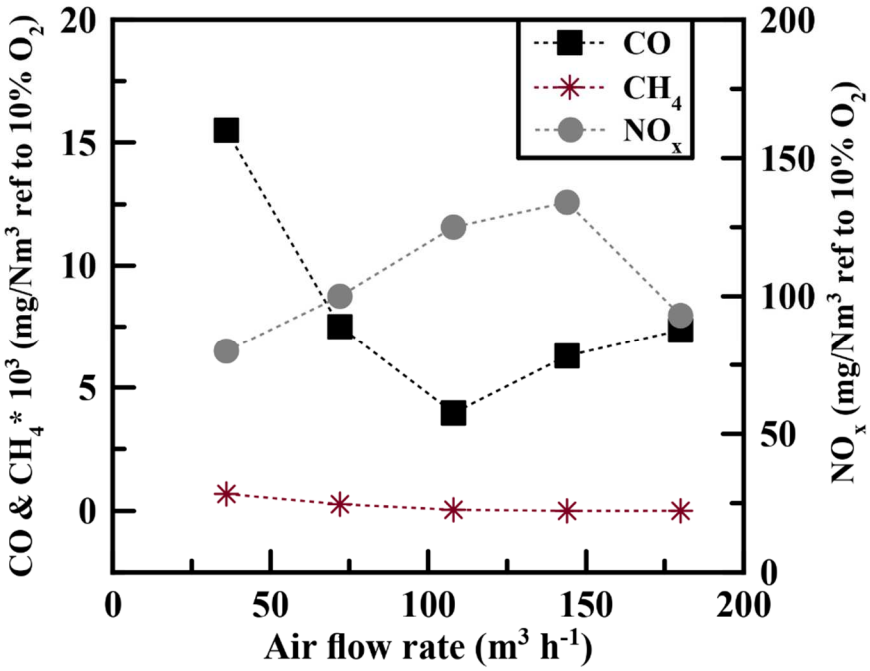

Fig. 8. Mean emission concentration during combustion corrected at 10% O_2.

It is concluded in this first part that the optimal air supply for the fixed-bed combustion of 1 kg of raw ANS was around 108 m^3.h^{-1}, which provided the highest flame and exhaust gas temperatures (886 and 698 °C, respectively), the highest FBR and BBV (1.39 g s^{-1} and 1.35 mm^2 s^{-1}, respectively), the highest MCE (97 %) and lower concentrations of pollutant (especially CO). In this case, the ash mass was the lowest (<1%) among the other air flows applied, indicating that practically all the biomass was burned.

3.4. Effect of particle size

The ANS biomass was classified into three different ranges of lengths: large (2.5-3 cm), small (1-1.5 cm) and broken (< 8 mm). Table 3 displays photographs and the calculated bulk densities (BD) of each classified sample.

Table 3 Classification of the three sizes from the raw ANS samples. Wood pellets are added for comparison purposes.

Samples	Large particles (LP)	Small particles (SP)	Broken particles (BP)	Wood pellets (WP)
photograph				
Length	2.5 – 3 cm	1 – 1.8 cm	< 8 mm	3.15 – 4 cm
BD*	556	592	642	650
Bed porosity	0.48	0.44	0.39	0.47

* BD: bulk density ($kg.m^{-3}$). Measurement was done in quadruplicate, and the mean value is reported.

Fig. 9a-f presents the effect of varying ANS length on combustion temperatures, FBR, MCE, and CO and NO_x emissions (corrected at 10% O_2). For each case, the performances were assessed at three constant air flows of 72, 108 and 180 $m^3.h^{-1}$, corresponding to weak, appropriate and excess air conditions, respectively (based on the results of raw ANS combustion). This can offer the possibility to investigate the effect of air flows and particle sizes at the same time. The results of raw ANS particles (RP) are included and a comparison with wood pellets is also reported. Fig. 9a and b show the influence of varying biomass length on the combustion temperature. For a low air supply (72 $m^3.h^{-1}$), the small particles (SP) generated the maximum flame temperature while the broken particles (BP) gave the minimum flame temperature. The results show that flame temperature increased from 834 to 900 °C when the broken particles (BP) were replaced by SP. The two other cases (LP and raw

355 particles) fell between the BP and SP. For the appropriate air supply (108 $m^3.h^{-1}$), the BP and
356 SP induced the same flame temperature, (910 °C), whereas the LP induced the minimum
357 flame temperature (858 °C) due to the short residence time in the combustion zone. Under
358 high excess air (180 $m^3.h^{-1}$), the difference in flame temperature was very high for the three
359 ANS sizes. For example, the flame temperature was 525 °C for LP and 952 °C for BP. Results
360 concerning the exhaust gas temperature (see Fig. 9b) exhibited the same evolution as that of
361 flame temperature. The exhaust gas temperatures of BP and WP were very close. Fig. 9c
362 shows that the FBR evolution with the air flow was similar for LP and SP. Depending on the
363 air supply, BP had the highest fuel burn rate compared to the other particle sizes and WP. The
364 LP and raw particle (RP) cases yielded the lowest FBR. In the case of the lower air flow, FBR
365 was 1.13, 1.15, 1.29, 1.45 and 1.40 g s^{-1} for RP, LP, SP, BP and WP respectively. These
366 values increased under moderate air flow (108 $m^3.h^{-1}$) to reach 1.39, 1.37, 1.49, 1.77 and 1.60
367 g s^{-1} for RP, LP, SP, BP and WP, respectively. Under a high air supply, the FBR decreased for
368 RP, LP and SP (1.35, 1.29 and 1.48 g/s, respectively) but continued to increase for BP and
369 WP (1.93 and 1.80 g s^{-1}, respectively). Fig. 9d presents the particle length effect on the
370 combustion efficiency. The MCE results of the different cases of ANS particle sizes are
371 completely different to the FBR results. The MCE value in the case of a 72 $m^3.h^{-1}$ air supply
372 was 94, 93, 80 and 84% for RP + LP, SP, BP and WP respectively. These values were found
373 to rise for all samples in the moderate air flow (108 $m^3.h^{-1}$) to reach 97, 96, 98, 81 and 91%
374 for RP, LP, SP, BP and WP, respectively. For the highest air supply (180 $m^3.h^{-1}$), MCE
375 declined for RP, LP and SP (93, 90 and 93%, respectively) but increased for the BP and WP
376 (90 and 97%, respectively). In the literature, some authors have studied the effect of biomass
377 size on combustion. El-Sayed et al. [24], found that the larger the size of the fuel particles, the
378 greater the probable residence time of the volatile gases within these particles. Ryu et al. [12]
379 proved that large particles (thermally thick) have a slow devolatilization rate and more

distributed heat transfer to the nearby particles. They noted that temperature gradients in the biomass bed during combustion decrease with increasing particle sizes. This led them to conclude that heat penetration to the cold particles below the hot ones is more extreme for smaller particles. Luo et al. [27] demonstrated that the biomass fuel burn rate and maximum combustion temperature increased with the decrease in particle size. The large particles present a greater resistance to heat transfer, and therefore their internal temperature was lower. In the present investigation, the optimal air supply for burning LP and SP was found to be similar to that needed for raw ANS particles (108 $m^3.h^{-1}$). Flame durations of 1kg ANS combustion were 681, 579 and 726s for 72, 108 and 180 $m^3.h^{-1}$, respectively in case of the LP. In the case of SP, the flame durations were 549, 558 and 628 for 72, 108 and 180 $m^3.h^{-1}$, respectively. These results agree with those of El-Sayed et al. [24]. RP, LP and SP showed the same behaviour for the three air flows used. They increased their performance when the air flow was changed from low (72 $m^3.h^{-1}$) to moderate (108 $m^3.h^{-1}$) conditions, but decreased regularly in higher air excess (180 $m^3.h^{-1}$). For the RP, LP and SP, 180 $m^3.h^{-1}$ is an excessive air flow during combustion, since it contributes to convective cooling of the biomass bed, slows down the process and extinguishes the flame (see Fig. 3). Contrariwise, the performance of BP and WP revealed an increasing trend when the air flow was increased. The FBR and the maximum combustion temperature of BP were the highest for the high air flows (108 and 180 $m^3.h^{-1}$) compared to the other sizes. This can be explained by the fact that when raw particles (RP) of ANS were broken, their contact area with air was greater, which leads to higher combustion reaction rates and greater air flow supply needs. The MCE value obtained for air flow rates of 72 and 108 $m^3.h^{-1}$ was low (the case of BP), indicative of a poor mixing process (high CO emissions) as indicated in Fig. 9e. However, an air flow of 180 $m^3.h^{-1}$ revealed a lower CO emission and a tolerable MCE value. Hence, it could be concluded that broken particles can be burned better than large particles and reach better combustion

performances if the required compromise of mixing air and biomass is achieved. The yields of NO_x emissions were found to be below 140 mg.Nm^{-3} for all the experimented conditions (see Fig. 9f). This was expected since fuel-N, considered as the major source of NO_x [28], was very low.

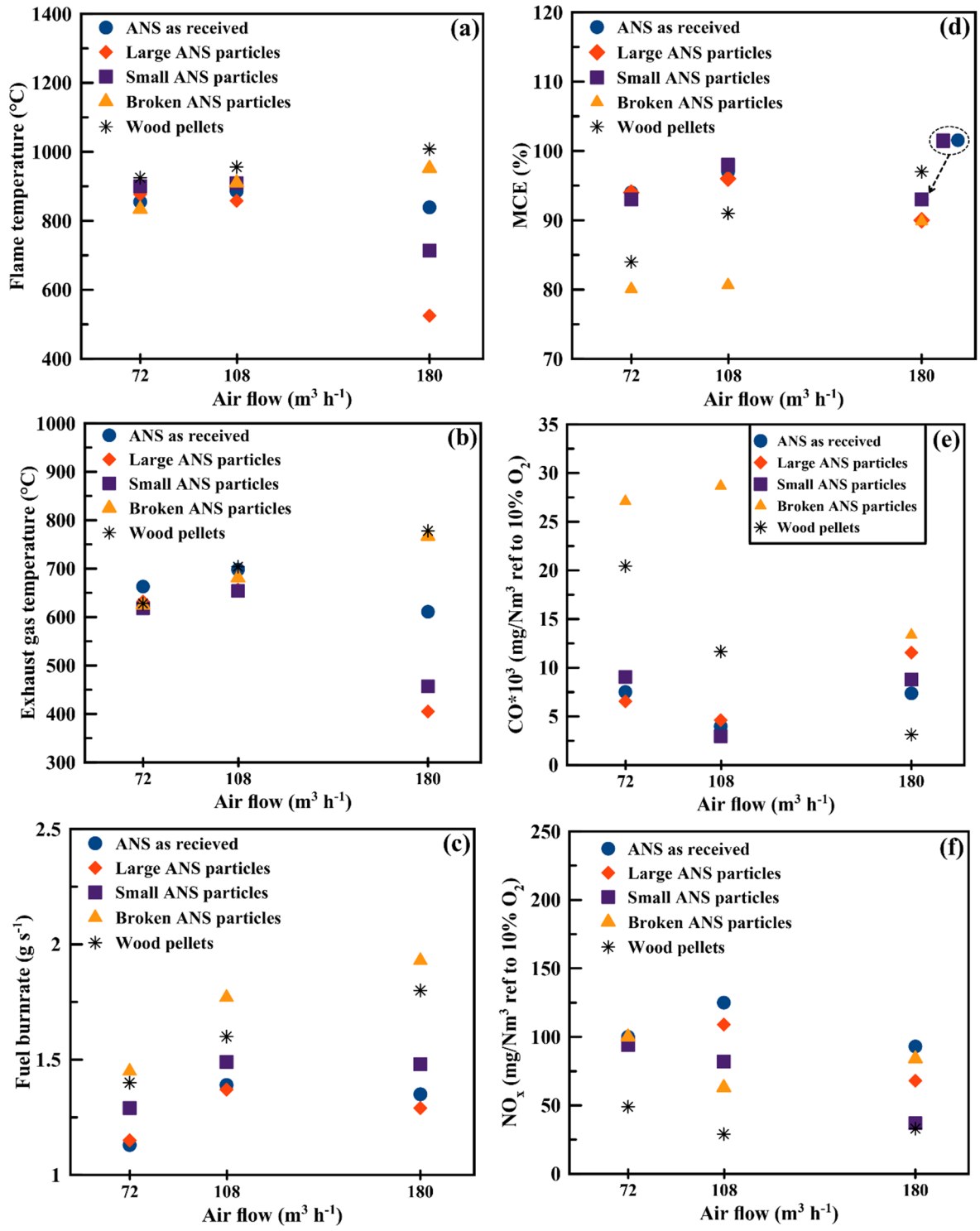

Fig. 9. Effect of particle size on combustion temperature (a and b), FBR (c), MCE (d), CO and NO_x emission (e and f, respectively).

3.5. Ash characterization

The ash of fixed beds of ANS is defined as the amount of solid residue that remains at the end of the combustion test. It is considered as a complex inorganic-organic mixture with a heterogeneous and variable composition [29]. Knowledge of the physicochemical properties of biomass ash is useful information in predicting the tendency to form deposits in boiler components. In this study, the ANS and WP ash produced during laboratory scale combustion included bottom and fly ash as shown in Fig. 10. In all the experiments, bottom ash represented the major part of total ash. Coarse particles of unburned char end up as bottom ash while finer ones flow out with gases in the form of fly ash. The colour of bottom ash ranged from light grey and brown to black. At first glance, one can see that the ash particles of raw ANS can be classified into three parts: unburned char marked by yellow diamonds (darker coloured biomass ash), incomplete char combustion marked by the red dotted circle, and totally combusted particles corresponding to the clearest particles (inorganic matter, particularly alkali and alkaline earth metals) marked by red circles in the corresponding figures. A high amount of unburned char was identified in the case of a low air supply (36 $m^3.h^{-1}$), indicating poor combustion efficiency. On the other hand, it can be seen that the residual bottom ash of WP was composed of solid parts (unburned biomass) which have the same colour as the raw sample (yellow square). The completely burned parts of WP are marked by a blue cross. The high unburned WP can be explained by the high biomass regime with an air supply of 72 $m^3.h^{-1}$. No clear sign of sintering and agglomeration was observed from the ANS ash displayed in Fig. 10a. Fly ash collected from the cyclone container was characterized by a black colour, i.e. a high-unburnt carbon content. Fig. 10b shows the

percentage mass (= $\frac{masse\ of\ ash}{initial\ mass\ of\ biomass\ bed}$ *100) of bottom and fly ash of ANS during combustion tests. It is observed that the bottom ash is generally low (<2%) except for raw, large and small particles under excess air conditions (C). This can be explained from the above results, which reveal that these kinds of particles have shown unstable combustion behaviour with limitations in flame mode. Therefore, the bottom ash is mainly generated by the quantity of unburnt particles as shown in the photos included in Fig.10b. The amounts of fly ash show an increasing trend with increasing air flow rate. The maximum fly ash content is observed for the broken particles at 180 $m^3.h^{-1}$. These particles with high air flow rate show stable combustion and well distributed flame throughout the bed. After the flame was extinguished, the oxidation of the char part, consisting of small particles, was very short, which favoured the transport of ash particles by the fumes. For a low air flow rate (A), fly ash is not detected.

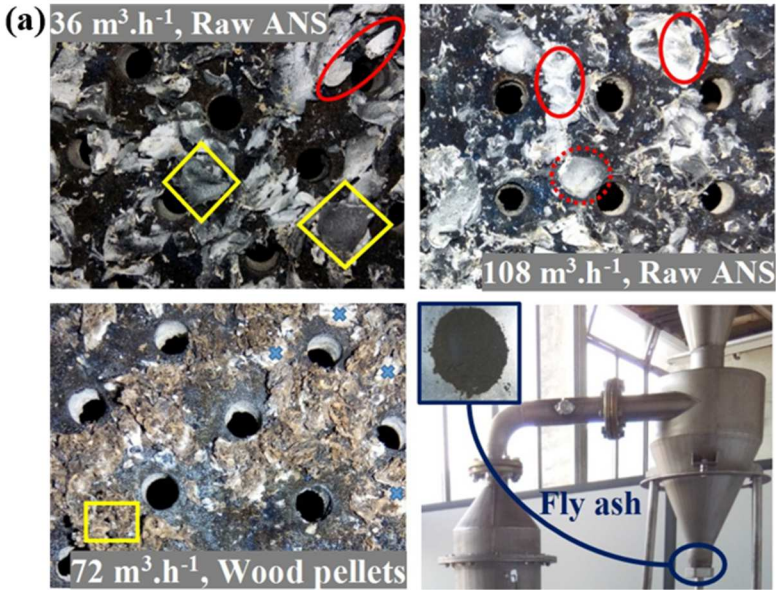

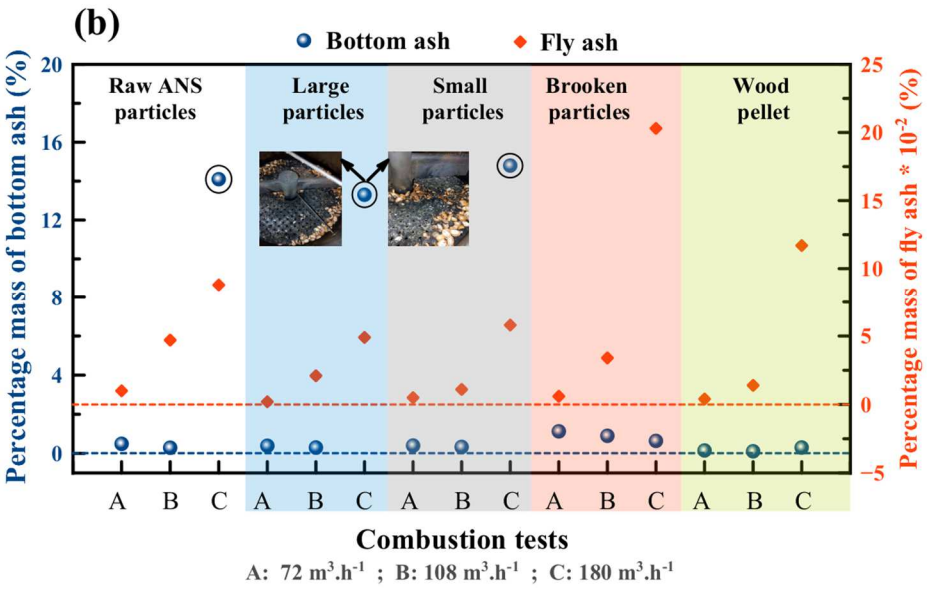

Fig. 10. Photographs of the ANS and WP combustion ashes in the grate (a) and the distribution of ash percentage mass during combustion tests (b).

SEM/EDS was used to analyse the residual ash of the studied samples by combining a visual image with elemental analysis. Fig. 11a-c illustrates the morphology of bottom ash from raw ANS and wood pellet samples at different operating conditions. Figures X, Y and Z show the zones marked in Fig. 11c at higher magnifications. The ash of BP of ANS was found to be mainly composed of unshaped particles and fine materials (Fig. 11a). These abundant unshaped particles showed a porous microstructure (Fig. 11b). Wood pellet ash showed mixed morphologies with particles of different shapes and sizes. In the X, Y and Z areas, the dominant number of unshaped materials in WP can be clearly seen (Fig. 11c). Fig. 11a-c also shows the selected areas indicated by crosses and rectangles (from 001 to 010) where the semi quantitative elemental analysis (atom %) was performed. The results of the ash analysis are summarized in Table 4. The morphology of ANS ash obtained during fixed-bed combustion was different from that obtained by LOI (see Fig. 4). No visible aggregation or crystal particles were observed. The porous structure (spots 1 and 4) was mainly composed of carbon (76 %), oxygen (18%) and potassium (5%). Other elements were found in minor amounts (Na, Mg and Ca). The Cl and Al percentage in the bottom ash samples was negligible. WP ash (see Fig. 11c) also contained significant quantities of carbon and oxygen. Ca, K, P and

Mg were detected as major elements (>1%), and Na, Si and Al as minor elements (<1%). S and Cl elements were not detected. The alkaline index (AI) is the amount of alkaline oxide in the biomass per unit of energy (kg alkaline per GJ). It was used in this study as an indicator of fouling and slag formation. The existence of such problems is likely for an AI greater than 0.17 $kg.GJ^{-1}$ and certain for a value greater than 0.34 $kg.GJ^{-1}$ [8,12,30]. Fixed-bed combustion of ANS gave an alkaline index of 0.17 $kg.GJ^{-1}$ and did not contribute to agglomeration. For WP a low AI value was obtained (0.05 $kg.GJ^{-1}$). In other terms, proximate analysis of ANS reveals a very low ash content (<1.5 %). During combustion, the obtained smaller particle size of ash (with no agglomeration) can be justified by the low temperature operation of the boiler (<1000°C). Additionally, the obtained low values of Na and Cl (minor elements: generally, <1%) in ANS ash are a good indicator for limiting the tendency of producing agglomerates. This can be justified with the fact that higher percentages of chloride (NaCl) contribute in a low ash-melting temperature, as reported in [31].

Fig. 11d-f shows the morphology of ANS and WP fly ash. Local chemical composition (spot I-XI) was carried out by EDS and the results are also summarized in Table 4. The ANS fly ash examined (Fig. 11d and e) mainly contained particles of various shapes and sizes. In general, prismatic, polyhedral, spherical and fibrous particles were observed. Coarse particles (spots II and III) with high specific surfaces represented typical organic materials. On the contrary, the fine particles were roughly spherical (dotted red circles) and mainly contained O, K, Si and Ca, while the amount of unburned carbon was minimal. Elemental concentrations of P, Na, Mg, Al and S were considerably lower than those of other elements. WP Fly ash (see Fig. 11f) mostly contained coarse and other fibrous particles resembling the original structure of wood fibre. The dark and fibrous particles were mainly formed of carbon and oxygen and came mainly from the unburnt char. In addition, the clearest and brightest particles were composed of inorganic materials, in particular alkali (K) and alkaline earth (Ca), as well as S

and Cl (as minor elements: 0.1-1%). The large amount of unburnt carbon in ANS and WP fly ash is mainly due to incomplete combustion of the char part. After flame extinction, the primary air cools the combustion chamber and transports the fine particles of char to the cyclone. Finally, under the moderate air flow (108 $m^3.h^{-1}$), the bottom and fly ash content of ANS were negligible (<0.5 and <0.05%, respectively), i.e. losses due to unburnt carbon can be neglected.

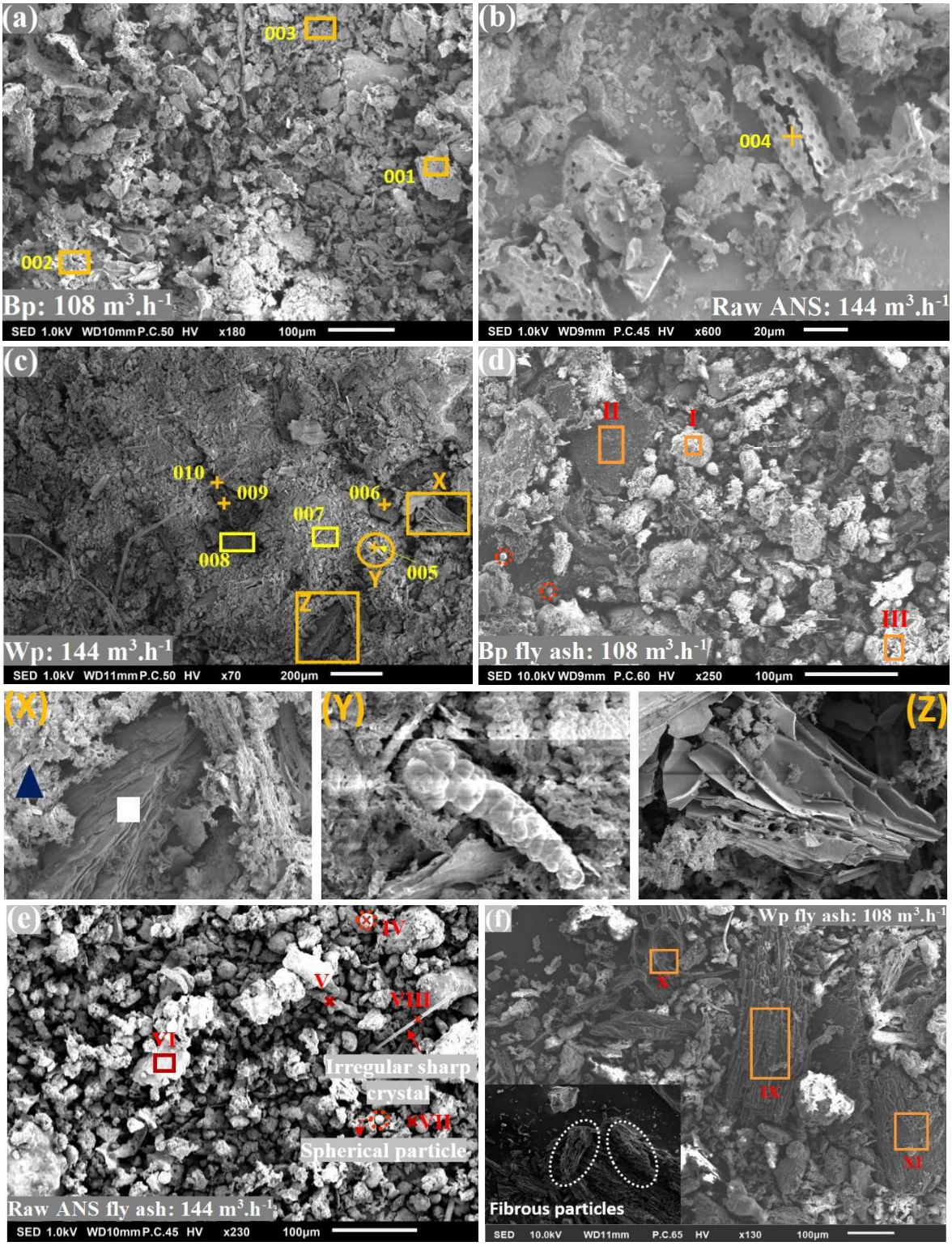

Fig. 11. SEM images of ANS and WP ash at different operating conditions: bottom ash (a-c) and fly ash (d-f).

Table 4 EDS analysis (atom %) of ANS and WP ash.

EDS		P	K	O	C	Na	Mg	Al	Si	S	Ca	Cl
Bottom ash												
Spot 1		-	4.53	19.5	73.9	0.84	-	-	-	-	1.2	-
Spot 2		0.36	15.6	50.4	15.8	15.2	0.31	0.21	-	-	1.9	0.3
Spot 3		0.6	11.9	18.3	67.6	0.9	-	-	-	-	-	0.64
Spot 4		-	5.05	15.7	78	0.8	-	-	-	-	-	-
Spot 5		-	4.3	28.3	67.4	-	-	-	-	-	-	-
Spot 6		0.8	2.4	27.4	51	-	2.7	-	-	-	15.8	-
Spot 7		1.8	24.7	39.8	17.6	0.4	2.4	0.4	0.6	-	12.5	-
Spot 8		0.6	10.6	22.3	58.9	-	1	-	-	-	6.61	-
Spot 9		-	11.6	-	88.4	-	-	-	-	-	-	-
Spot 10		9.5	3.9	34.3	10.2	-	5.4	0.6	0.9	-	35.2	-
Fly ash												
Spot I		0.74	23.54	16.60	30.18	1.86	0.97	3.44	-	1.28	3.04	18.36
Spot II		0.49	8.98	17.86	61.23	1.58	-	-	-	2.67	2.39	4.79
Spot III		0.50	18.28	41.71	16.20	11.87	-	0.33	-	1.03	6.09	4.01
Spot IV		0.76	10.67	44.29	12.56	2.65	-	-	17.84	0.51	10.09	0.64
Spot V		7.59	6.39	34.49	21.68	1.30	2.11	1.65	5.22	0.78	16.51	2.28
Spot VI		0.49	36.80	23.02	4.18	0.46	-	10.61	14.28	1.22	-	4.35
Spot VII		0.78	36.21	13.54	19.63	1.00	0.54	-	1.02	3.12	5.55	18.61
Spot VIII		-	4.82	19.98	20.41	0.67	1.61	-	24.78	0.69	25.30	1.66
Spot IX		-	3.19	15.73	78.64	-	-	-	-	0.66	1.10	0.68
Spot X		-	7.32	14.47	76.36	-	-	-	-	-	1.86	-
Spot XI		-	6.66	19.18	71.91	-	-	-	-	-	-	-
Window (a)	*	0.5	10.6	29.4	52.4	5.7	0.3	0.2	-	-	1.5	0.5
	**	0.2	5.6	18.2	31.9	8.2	0	0			0.5	0.2
	A.I	0.17 (Kg alkaline/GJ)										
Window (b)	A.I	0.06 (Kg alkaline/GJ)										
Window (c)	*	3.2	9.6	30.4	48.9	0.4	2.9	0.5	0.7	-	17.1	-
	**	4.3	8.3	6.7	30	0	1.9	0.2	0.2		12.9	
	A.I	0.05 (Kg alkaline/GJ)										

* Average, ** Deviation

4. Conclusion

The understanding of biomass combustion behaviours, performances and their environmental impact is a crucial consideration in terms of sustainable energy development. For this purpose, the most frequent biomass in southwestern Morocco, namely argan nut shell (ANS), was studied. Many conclusions can be drawn based on the experimental results of this work. ANS was burnt in the laboratory furnace without any ash agglomeration problem. On increasing the air flow, the combustion temperature, the FBR and the MCE of raw ANS increased until a critical value which corresponds to 108 $m^3.h^{-1}$ in our study. At this air flow rate, less CO concentration is obtained and the ash content is almost negligible. High air

excess reduces the reaction time and consequently the flame temperature and the combustion efficiency since the carbon conversion was limited. With the decrease in ANS length, the combustion duration was shorter, which results in a rise in the FBR. However, the shortest ANS biomass length (broken particles: BP) induced high CO concentration and consequently lower MCE under low and moderate air flows (72 and 108 $m^3.h^{-1}$, respectively). A high excess of air supply, especially for the BP improved the FBR (better than wood pellets), the combustion temperature, the emission of CO and the MCE. In all the cases studied, the average NO_x emission was less than 140 $mg.Nm^{-3}$ at 10% O_2. The flame had an irregular shape for the longest ANS biomass but was more stable when the biomass particle size decreased (BP). These facts indicate that a change in fuel specification clearly affects the combustion process. Such results prove that ANS biomass may be an alternative fuel for present and future energy production. Nevertheless, further work is required to study the effect of secondary air on pollutant emissions (especially CO) of BP of ANS to ensure their suitability for combustion. This will not only give further information on the combustion characteristics of this biomass but also validate the presented results in this study.

Nomenclature

ANS	Argan nut shell
RP	Raw particles
LP	Large particles
SP	Small particles
BP	Broken particles
WP	Wood pellet
M	Moisture content (wet %)
VM	Volatile matter (wet %)
FC	Fixed carbon (wet %)

BD	Bulk density ($kg.m^{-3}$)
LHV	Low heating value ($MJ.kg^{-1}$)
ED	Energetic density ($GJ.m^{-3}$)
AFR	Air fuel ratio (kg air/kg fuel)
TC	Thermocouple
FBR	Fuel burn rate ($kg.s^{-1}$)
MCE	Modified combustion efficiency (%)
BBV	Biomass bed velocity ($mm^2.s^{-1}$)
SEM	Scanning electron microscopy
EDS	Energy dispersive x-ray spectroscopy
AI	Alkaline index ($kg.GJ^{-1}$)

Acknowledgements

This work has been supported by the ANR (Agence National de la Recherche), EranetMed II RenewValue project. The technical help of Radouane Leghrib from LETSMP Ibn Zohr University is gratefully acknowledged.

References

[1] T. Kousksou, A. Allouhi, M. Belattar, A. Jamil, T. El Rhafiki, A. Arid, Y. Zeraouli, Renewable energy potential and national policy directions for sustainable development in Morocco, Renew. Sustain. Energy Rev. 47 (2015) 46–57, https://doi.org/10.1016/j.rser.2015.02.056.

[2] M. Balat, G. Ayar, Biomass energy in the world, use of biomass and potential trends, Energy Sources. 27 (2005) 931–940. https://doi.org/10.1080/00908310490449045.

[3] J. Werther, M. Saenger, E.-U. Hartge, T. Ogada, Z. Siagi, Combustion of agricultural residues, Prog. Energy Combust. Sci. 26 (2000) 1–27. https://doi.org/10.1016/S0360-1285(99)00005-2.

[4] F.Z. Zouhair, A. Benali, M.R. Kabbour, K. EL Kabous, E. haj El Maadoudi, M. Bouksaim, A. Essamri, Typical characterization of argane pulp of various Moroccan areas: A new biomass for the second-generation bioethanol production, J. Saudi Soc. Agric. Sci. (2018). https://doi.org/10.1016/j.jssas.2018.09.004.

[5] Nussbaumer Thomas, Combustion and Co-combustion of Biomass: Fundamentals, Technologies, and Primary Measures for Emission Reduction, Energy and Fuels. 17 (2003) 1510–1521. https://doi.org/10.1021/ef030031q.

[6] A.K. Asthana, Biomass as fuel in small boilers, 2009. www.apo-tokyo.org.

[7] S. Khlifi, M. Lajili, F. Tabet, T. Boushaki, B. Sarh, Investigation of the combustion characteristics of briquettes prepared from olive mill solid waste blended with and without a natural binder in a fixed bed reactor, Biomass Convers. Biorefinery. (2019). https://doi.org/10.1007/s13399-019-00449-7.

[8] A. Khor, C. Ryu, Y. bin Yang, V.N. Sharifi, J. Swithenbank, Straw combustion in a fixed bed combustor, Fuel. 86 (2007) 152–160. https://doi.org/10.1016/j.fuel.2006.07.006.

[9] Z. Cepic, B. Nakomcic-Smaragdakis, B. Miljkovic, L.Z. Radovanović, S. Djuric, Combustion characteristics of wheat straw in a fixed bed, Energy Sources, Part A Recover. Util. Environ. Eff. 38 (2016) 1007–1013. https://doi.org/10.1080/15567036.2014.922646.

[10] M.M. Roy, A. Dutta, K. Corscadden, An experimental study of combustion and emissions of biomass pellets in a prototype pellet furnace, Appl. Energy. 108 (2013) 298–307. https://doi.org/10.1016/j.apenergy.2013.03.044.

[11] Y. Elmay, G. Trouvé, M. Jeguirim, R. Said, Energy recovery of date palm residues in a domestic pellet boiler, Fuel Process. Technol. 112 (2013) 12–18. https://doi.org/10.1016/j.fuproc.2013.02.015.

[12] C. Ryu, Y. Bin Yang, A. Khor, N.E. Yates, V.N. Sharifi, J. Swithenbank, Effect of fuel properties on biomass combustion: Part I. Experiments - Fuel type, equivalence ratio and particle size, Fuel. 85 (2006) 1039–1046. https://doi.org/10.1016/j.fuel.2005.09.019.

[13] Y. Rahib, T. Boushaki, B. Sarh, A. Ihlal, J. Chaoufi, S. Bonnamy, A. Elorf, Combustion analysis of fixed beds of argan nut shell (ANS) biomass in batch type reactor, 2019 7th International Renewable and Sustainable Energy Conference (IRSEC), Agadir, Morocco, 2019, pp. 1-7, https://doi.org/10.1109/IRSEC48032.2019.9078217.

[14] T. Onabanjo, A.J. Kolios, K. Patchigolla, S.T. Wagland, B. Fidalgo, N. Jurado, D.P. Hanak, V. Manovic, A. Parker, E. McAdam, L. Williams, S. Tyrrel, E. Cartmell, An experimental investigation of the combustion performance of human faeces, Fuel. 184 (2016) 780–791. https://doi.org/10.1016/j.fuel.2016.07.077.

[15] X. Meng, R. Sun, T.M. Ismail, W. Zhou, X. Ren, R. Zhang, Parametric studies on corn combustion characteristics in a fixed bed: Primary air flow rate and different corn lengths, Appl. Therm. Eng. 126 (2017) 702–716. https://doi.org/10.1016/j.applthermaleng.2017.07.197.

[16] Y. Rahib, B. Sarh, J. Chaoufi, S. Bonnamy, A. Elorf, Physicochemical and thermal analysis of argan fruit residues (AFRs) as a new local biomass for bioenergy production, J. Therm. Anal. Calorim. (2020). https://doi.org/10.1007/s10973-020-09804-7.

[17] TSI, Combustion Analysis Basics: An Overview of Measurements, Methods and Calculations Used in Combustion Analysis, 2004.

[18] R. García, C. Pizarro, A.G. Lavín, J.L. Bueno, Biomass sources for thermal conversion. Techno-economical overview, Fuel. 195 (2017) 182–189. https://doi.org/10.1016/j.fuel.2017.01.063.

[19] Y. Rahib, A. Elorf, B. Sarh, S. Bonnamy, J. Chaoufi, M. Ezahri, Experimental analysis on thermal characteristics of argan nut shell (ANS) biomass as a green energy resource, Int. J. Renew. Energy Res. 9 (2019) 1606–16015.

[20] Y. Rahib, B. Sarh, S. Bostyn, S. Bonnamy, T. Boushaki, J. Chaoufi, Non-isothermal kinetic analysis of the combustion of argan shell biomass, Mater. Today Proc. (2020) 11–16. https://doi.org/10.1016/j.matpr.2019.07.437.

[21] G. Leyssens, G. Trouvé, I. Caplain, C. Schönnenbeck, F. Cazier, Energetic performances and environmental impact of the combustion of cardboard/sawdust in a domestic boiler, Fuel. 122 (2014) 21–27. https://doi.org/10.1016/j.fuel.2014.01.034.

[22] S. Polesek-Karczewska, T. Turzyński, D. Kardaś, Heda, Front velocity in the combustion of blends of poultry litter with straw, Fuel Process. Technol. 176 (2018) 307–315. https://doi.org/10.1016/j.fuproc.2018.03.040.

[23] Y. Yuzuriha, W. Gao, T. Mogi, R. Dobashi, Effects of particle size distributions on flame propagation behavior through dust clouds of PMMA, J. Loss Prev. Process Ind. 49 (2017) 852–858. https://doi.org/10.1016/j.jlp.2017.06.011.

[24] S.A. El-Sayed, M. Khairy, An experimental study of combustion and emissions of wheat straw pellets in high-temperature air flows, Combust. Sci. Technol. 190 (2018) 222–251. https://doi.org/10.1080/00102202.2017.1381953.

[25] A.I. Calvo, L.A.C. Tarelho, C.A. Alves, M. Duarte, T. Nunes, Characterization of operating conditions of two residential wood combustion appliances, Fuel Process. Technol. 126 (2014) 222–232. https://doi.org/10.1016/j.fuproc.2014.05.001.

[26] G. Wielgosinski, P. Lechtanska, O. Namiecińska, Emission of some pollutants from biomass combustion in comparison to hard coal combustion, J. Energy Inst. 90 (2017) 787–796. https://doi.org/10.1016/j.joei.2016.06.005.

[27] S. Luo, B. Xiao, Z. Hu, S. Liu, M. He, Experimental study on combustion of biomass micron fuel (BMF) in cyclone furnace, Energy Convers. Manag. 51 (2010) 2098–2102. https://doi.org/10.1016/j.enconman.2010.03.001.

[28] H. Khodaei, F. Guzzomi, D. Patiño, B. Rashidian, G.H. Yeoh, Air staging strategies in biomass combustion-gaseous and particulate emission reduction potentials, Fuel Process. Technol. 157 (2017) 29–41. https://doi.org/10.1016/j.fuproc.2016.11.007.

[29] U. Kleinhans, C. Wieland, F.J. Frandsen, H. Spliethoff, Ash formation and deposition in coal and biomass fired combustion systems: Progress and challenges in the field of ash particle sticking and rebound behavior, Prog. Energy Combust. Sci. 68 (2018) 65–168, https://doi.org/10.1016/j.pecs.2018.02.001.

[30] T. Blomberg, Free alkali-index for optimizing the fuel mixture in biomass co-firing, Heat Exch. Fouling Clean. VII. (2007) 14.

[31] M. Brostrom, S. Enestam, R. Backman, K. Mäkelä, Condensation in the KCl-NaCl system, Fuel Process. Technol. 105 (2013) 142–148. https://doi.org/10.1016/j.fuproc.2011.08.006.